Egyptian Journal of Petroleum (2015) **24**, 163–174

HOSTED BY

Egyptian Petroleum Research Institute

Egyptian Journal of Petroleum

www.elsevier.com/locate/egyjp
www.sciencedirect.com

FULL LENGTH ARTICLE

Influence of Pt nanoparticles modified by La and Ce oxides on catalytic dehydrocyclization of *n*-alkanes

A.H. Samia [a], M.S. Mohammed [a,*], S. Faramawy [a], S.A. Ahmed [a], H.B. Ahmed [b]

[a] *Egyptian Petroleum Research Institute, Nasr City 11727, Cairo, Egypt*
[b] *Faculty of Science, AL-Azhar University, Cairo, Egypt*

Received 25 January 2014; accepted 6 April 2014
Available online 15 June 2015

KEYWORDS

Dehydrogenation;
Dehydrocyclization;
La, Ce promotion;
Pt/Al_2O_3;
Characterization

Abstract Catalytic reforming accounts for a large share of the world's gasoline production, it is the most important source of aromatics for the petrochemical industry. In addition, reforming of hydrocarbon on the dual-function catalysts has been found to form fundamentally different products in hydrogen diluents. Typical catalysts employed for this reforming process are Pt/Al_2O_3 and $Pt\text{-}M/Al_2O_3$, M being the promoter. These solids are characterized by both acid and metal functions which catalyze dehydrocyclization, dehydrogenation, isomerization and cracking processes. In this regard, information about cerium and lanthanum, as promoters, is hardly revealed. The present work aims to study the performance of Pt/Al_2O_3 catalysts modified by lanthanum or cerium during the conversion of cyclohexane, *n*-hexane and *n*-heptane. Catalytic activities of the prepared catalysts were tested using a micro catalytic pulse technique. Physicochemical characterization of the solid catalysts such as, surface area (S_{BET}), Fourier transform infrared (FTIR), differential scanning calorimetry (DSC), thermogravimetric analysis (TGA), hydrogen-temperature programed reduction (H_2-TPR), hydrogen-temperature-programed desorption (H_2-TPD), CO_2-TPD, NH_3-TPD, high resolution transmission electron microscopy (HRTEM) and X-ray diffraction (XRD) were depicted. Results indicated clearly that Pt/Al_2O_3 catalyst is selective toward dehydrogenation to benzene which could be explained as due to the decrease in the active acid sites and the comparative segregation of the alumina support especially at 3% load of CeO. The presence of La_2O_3 in the Pt/Al_2O_3 catalyst promotes aromatization of *n*-hexane and *n*-heptane, also the dehydrocyclization of *n*-hexane is more difficult than that of *n*-heptane. Thus, modification of the Pt/Al_2O_3 catalyst by La, resulted in a more active and selective reforming catalyst.

1. Introduction

Many feedstock sources, including condensate or natural gasoline, are attractive reforming feed [1]. Condensate is a large source of potential feedstock for aromatics production and may contain alkanes, naphthenes and aromatics. Although

* Corresponding author.
Peer review under responsibility of Egyptian Petroleum Research Institute.

http://dx.doi.org/10.1016/j.ejpe.2015.05.007

most condensate is currently used as cracker feedstock to produce ethylene, condensate will likely play an increasingly important role in aromatics production in the future.

Many efforts have been made to improve the catalytic performance of platinum-based catalysts. The addition of a second specific metal or metal oxide can improve the activity and/or selectivity toward the desired product [2]. The rare earth elements (RE), due to their excellent electronic properties, are widely used in the form of oxides for the modification and promotion of catalyst activity [3].

In the case of metal based catalysts the effect of RE elements was promoters that lead to metal dispersion and thermal stability elevator of the support [4]. In fact, the goal of reducing the amount of noble metals present in industrial catalysts, appeals for the use of RE on metal loaded catalyst. Automotive exhaust catalysts are an example of catalyst improvement upon the introduction of small amounts of RE elements and their influence as on bi-functional catalysts [5]. The effect of RE addition on platinum supported KL Zeolite, during catalytic reforming processes, was also reported as effective against sulfur poisoning resistance and as reported by Fang et al. [6]. Pt is rarely used in the pure state but is more often used in modern catalysts in the presence of the so-called ''promoters''. Promoted catalysts are considered more selective and stable than pure Pt supported catalyst when operated under less severe reaction conditions (lower pressure, lower hydrogen-to hydrocarbon ratio). The catalytic properties of the Pt M supported catalysts, (M = promoter), strongly depend on the interaction between Pt and M. Rare earth elements, such as lanthanum and cerium, who acquire unique thermal stabilization properties such as that described for alumina support due to strong metal-rare earth oxide interactions [7]. Accordingly, the promotion effects of cerium or lanthanum on the catalytic performance of Pt/Al_2O_3 catalyst are expected to motivate the catalytic behavior of noble metal supported catalysts. The present work aims at studying the effect of La and Ce addition, as promoters, to Pt/Al_2O_3 acidity and textural alterations and therefore their direct effect on the catalytic conversion and selectivity of dehydrocyclization of *n*-alkanes at different load contents.

2. Experimental

2.1. Chemicals

Boehmite [Chemical Formula: AlO(OH)] from Prolabo, $La(NO_3)\cdot 6H_2O$, $Ce(NO_3)\cdot 6H_2O$, $H_2PtCl_6\cdot 6H_2O$ and citric acid all from Merck., cyclohexane, *n*-hexane and *n*-heptane; all from Aldrich.

The γ-Al_2O_3 support was prepared by drying Boehmite at 120 °C overnight and then calcination at 550 °C, in air for 4 h.

2.2. Catalyst preparation

The reference Pt (0.35 wt.%)/Al_2O_3 catalyst was prepared by wet impregnation of the γ-Al_2O_3 support with appropriate concentration of Pt precursor ($H_2PtCl_6\cdot 6H_2O$) aqueous solution to achieve 0.35 wt.%/Pt. A small amount of citric acid was added to the Pt precursor solution to improve the penetration of the Pt into the alumina support particles to achieve optimum dispersion of the metal and as reported by Ahmed et al. [8]. The sample was then dried at 120 °C overnight and finally calcined at 550 °C in air for 4 h.

Promoters, i.e., La and Ce, were added to Pt/γ-Al_2O_3 by successive impregnation at appropriate amounts of La, or Ce precursor aqueous solution to acquire loads of 0.25, 1.5, and 3 wt.%. The final product samples were dried and calcined as described earlier. All the prepared catalysts were at fixed Pt content of 0.35 wt.%. Catalyst samples designation is referred to as in Table 1.

Prior to catalytic reaction, an ex-situ reduction in flowing H_2 (20 ml min^{-1}) at 500 °C for 4 h and an in situ reduction at 500 °C for 1 h in 20 ml min^{-1} of H_2 flow was performed. During reduction, the temperature increase rate was 8 °C min^{-1} in each case.

2.3. Support and catalysts characterization

The elemental analysis of La, Ce, and Pt contents was performed through X-ray fluorescence (XRF) using channel control PW 1390-Philips and spectrometer PW1410 whereby the content of each element is ensured according to desired permutation prior to use.

X-ray powder diffraction (XRD) patterns using Brucker AXSD 8 Advance (Germany) employing nickel-filtered copper radiation ($\ddot{e}$ = 1.5405 Å) at 60 kv and 25 mA with a scanning speed of 8 °C over 20 min^{-1} were considered for crystallinity studies. Surface area and pore volumes of the support and catalyst materials were determined using USA Nova 3200 apparatus. The chemical structure was elucidated through the use of ATI Mattson Genesis, 960 M009 series FT-IR (KBr disk method) Thermal behavior (DSC and TGA) of the solid samples was examined using SDT-Q600 thermogravimetic apparatus. Hydrogen-temperature-programed reduction (H_2-TPR) for precursor catalysts were carried out from ambient to 1000 °C, with a flow of 10% H_2/N_2 (85 ml min^{-1}) at a heating rate of 10 °C min^{-1} using Chembet 3000 analyzer and were carried out in the same setup as TPR. Before H_2-TPD experiments are carried out, the solid samples of 0.2 g were reduced under flowing pure H_2 at 576 °C for 2.5 h. After reduction, the solid catalyst was cooled to 25 °C in the flowing H_2. The gas stream was replaced by Argon gas and subsequently a TPD experiment was performed (10 °C min^{-1}) up to 540 °C. Basicity assessment of the solid samples was also carried out in order to relate the catalytic activity and its basic properties of the catalyst samples. TPD of CO_2 is frequently used to measure the basicity of catalysts. The number and strength of basic sites are evaluated from the intensity and position temperature

Table 1 Chemical and textural characteristics of the catalysts.

Catalyst	Loading (wt.%)			Surface area (m^2/g)	Pore volume (cm^3/g)
	Pt	La	Ce		
Pt/A*	0.35	—	—	260	0.60
PtLa(0.25)/A*	0.35	0.25	—	261	0.28
PtLa(1.5)/A*	0.35	1.5	—	243	0.26
PtLa(3)/A*	0.35	3	—	227	0.25
Pt Ce(0.25)/A*	0.35	—	0.25	270	0.26
Pt Ce(1.5)/A*	Pt	—	1.5	226	0.24
Pt Ce(3)/A*	0.35	—	3	221	0.23

* γ-Al_2O_3

of TPD signals. To assess the acidity of the different catalysts NH_3-TPD adsorption/desorption was followed using the same apparatus. Solid catalyst particle size and features were conducted through high resolution transmission electron microscopy (HR-TEM) using Jeol/JEM 2100, 200 kv.

2.4. Catalytic activity measurement

Catalytic activity assessment of the prepared catalyst samples (0.20 g) was revealed through its application of cyclohexane, *n*-hexane and *n*-heptane conversion, as model compounds of cyclo-paraffins and n-paraffins, using the micro catalytic pulse technique. The reactants were injected in micro quantities (2 μl) by micro syringe in the form of pulses. Reactants and products were analyzed with an online gas chromatograph. Computerized data acquisition system, model 201 24-Bit (Italy) was used for integrating and recording the effluent yield. The reaction was carried out under atmospheric pressure and a temperature range of 300–450 °C at a constant hydrogen flow of 20 ml/min^{-1}. Prior to the catalytic activity test, the reduced catalyst samples were heated in H_2 flow up to 500 °C with a heating rate of 8 °C min^{-1} and kept at 1 h at 500 °C for their activation. Few doses of reactants were injected first to reach a steady state of activity. The gas chromatograph column used was 200 cm in length and 0.3 cm in diameter, packed with Chromosorb AW (80–100 mesh size) from Merck, loaded with 15 wt.% Squalan (Merck). The chromatographic column temperature was adjusted and controlled at 70 °C.

3. Results and discussion

3.1. Catalyst characterization

3.1.1. XRF-XRD

X-ray fluorescence (XRF) was used to monitor the required wt.% of La, Ce, and Pt of catalysts. XRD analysis is presented in Fig. 1. As revealed only the diffraction peaks that correspond to γ-Al_2O_3 were observed but distinct peaks that correspond to either the metallic platinum or the rare earth were not observed may be due to their low concentration and their diffusion and inclusion in the alumina matrix without affecting the alumina matrix agglomeration mode or incapability to rearrange its characteristic agglomeration phase [13]. Such elucidation is supported by HRTEM images, where particles grain size of alumina support seems unchanged upon loading with the noble metal or the rare earth elements, Fig. 9, indicating alumina structural sustainability even upon loading of limited loading of sizable foreign elements.

3.1.2. Structural characterization

Surface area and pore volume of Pt/Al_2O_3, La, and Ce promoted catalysts after calcinations at 550 °C are summarized in Table 1. The surface area of samples with lower La_2O_3 and CeO_2 content (0.25 wt.%) is observed as slightly higher in value than those of the unpromoted catalyst. However, higher La_2O_3 and CeO_2 loadings (>0.25%) lead to a significant decrease with regard to the surface area and pore volume may be due to blocking of the pores by promoter oxide species, thus influencing the thermal stability of alumina [9]. It has been reported that low rare earth oxide loading could stabilize γ-Al_2O_3 against surface area loss by preventing the agglomeration of Al_2O_3 particles, the transformation of γ-Al_2O_3 to k-Al_2O_3 and hinders platinum sintering upon calcination treatment of the catalyst [10]. Over Pt-Ce/γ-Al_2O_3 catalyst, the strong interaction between Ce and alumina results in the formation of surface Ce Al_2O_3 by Ce^{3+} cation occupying the vacant octahedral sites on the alumina surface. This initial occupation of octahedral sites by cerium cations blocks the transition of Al^{3+} cations from tetrahedral to octahedral sites during high temperature treatment which causes the loss of the surface area of alumina [9,10].

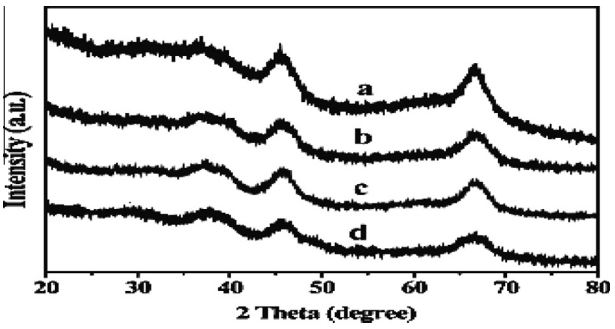

Figure 1 XRD patterns of (a) the support Al_2O_3, (b) Pt(0.35)/Al_2O_3, (c) Pt (0.35) Ce (3)/Al_2O_3 and (d) Pt (0.35)La(3)/Al_2O_3 samples.

3.1.3. Thermal characterization

Evaluation of weight loss, rate of weight loss as well as the heat effects associated with heating the sample from room temperature up to 1000 °C (with a heating rate of 10 °C min^{-1}) is important, because it enables us to determine the maximum temperature after which the catalyst weight loss is negligible (i.e., complete decomposition). This, in turn, allows establishing the minimum temperature at which the catalyst becomes thermally stable, and as such, the minimum temperature for catalyst calcinations. TGA profiles for the dried samples are shown in Figs. 2 and 3. The profiles indicates a two-stage weight loss at 90 °C which is attributed to the loss of physisorbed water and that at 550 °C is attributed to the elimination of the hydroxylic water and precursor salt oxidation to the oxide compound formation. At temperatures above 550 °C a slow and gradual loss of mass was observed which can be attributed to the continuous release of residual traces of hydroxylic H_2O and that of the metal oxide precursor salt. DSC profile of parent alumina, Fig. 2a, reflects such behavior upon thermal treatment exhibiting two types of endothermic and exothermic features. The first endothermic appeared at 83 °C, this peak is related to the removal of physisorbed water covering the surface. The second endothermic peak that appeared at 275 °C is related to various endothermic transitions, i.e., the losses of chemically bound water and departure of the hydroxide precursor may still be contaminated with the precipitated materials [11]. The two exothermic behaviors around 450 and 875 °C correspond to crystallization of γ-Al_2O_3 and k-Al_2O_3, respectively [12].

The thermal behavior profile of Pt/Al_2O_3 catalyst shown in Fig. 2b reveals that no variation compared to γ-Al_2O_3 occurs due may be to the low platinum loading. Upon addition of

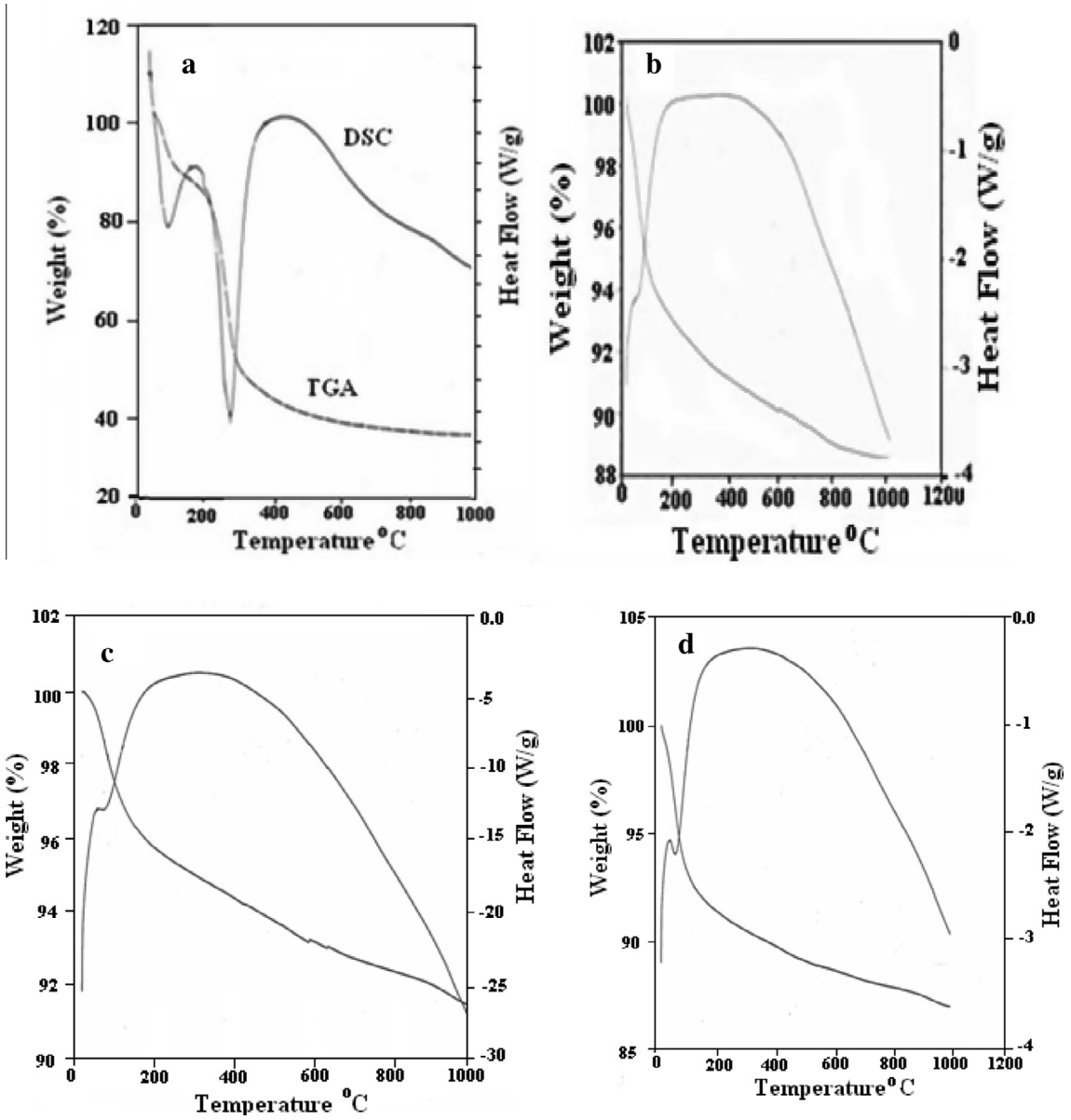

Figure 2 TGA and DSC profiles of: (a) γ-Al_2O_3 support; (b) Pt/Al_2O_3 catalyst; (c) Pt La (0.25 wt.%)/Al_2O_3 catalyst; (d) Pt La (3 wt.%)/Al_2O_3 catalyst.

La_2O_3, the thermal stability of γ-Al_2O_3 was noticed to increase may be due to the dispersion of the promoter particles within the alumina and its direct impact on its thermal properties, Fig. 2a and b. Cerium promoted catalyst, Fig. 3b, exhibits an emerging new exothermic peak around 550 °C in addition to the original exothermic peak characterizing Al_2O_3 oxide. The new exothermic peaks could be due to a segregation process of CeO_2 (3 wt.%). The elevated thermal stability of γ-Al_2O_3, upon the presence of La and Ce, is explained as due to the hindering of transformation to the less stable k-Al_2O_3 phase [10].

3.1.4. FT-IR

FT-IR examination was utilized to monitor any possible structural changes that could occur to the alumina support, Pt/Al_2O_3 and upon loading by of La, and Ce promoters, (Fig. 4). Pure γ-Al_2O_3 structure was regarded as hydrogen spinal and the complex Al-O IR absorption band between 1100 and 500 cm^{-1}, (Fig. 4a) and as reported [14]. The low frequency areas (500–680 cm^{-1}) should be dominated by the stretching vibration band of AlO_6 octahedral. The high frequency areas (680–1000 cm^{-1}) are associated due to the stretching vibration band of AlO_4 tetrahedral [15]. In addition, the γ-Al_2O_3 exhibits a new absorption band at 1406 cm^{-1} which could be assigned as due to the longitudinal acoustical mode vibration of the nano-γ-Al_2O_3 [16]. Alumina possess well-defined hydroxyl bands whose nature and intensity are affected by alumina impurity content [17]. Broad intense bands between 3600 and 3300 cm^{-1} are mainly due to the –OH stretching mode of layer hydroxyl groups and interlayer water molecules. A shoulder band that appears at 3790 cm^{-1} is related to the terminal –OH groups situated over one

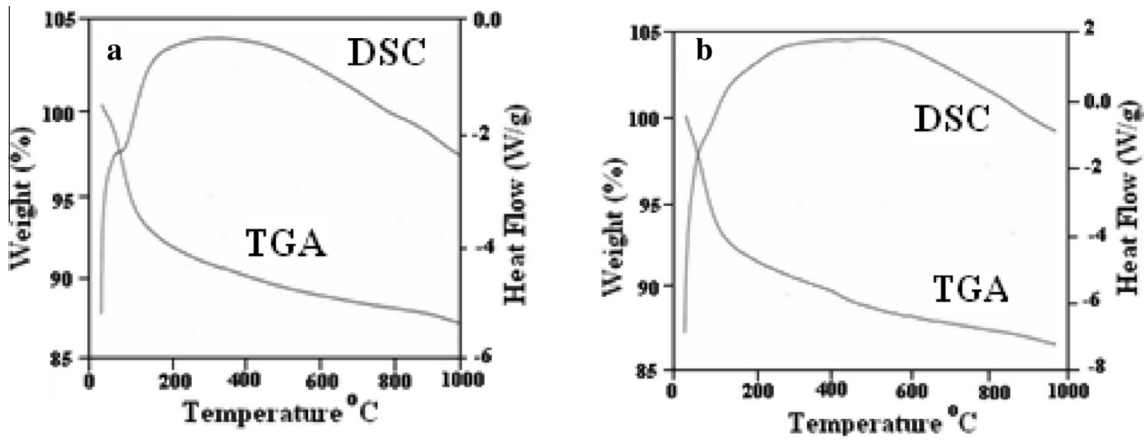

Figure 3 TGA and DSC profiles of: (a) Pt Ce (0.25 wt.%)/Al_2O_3 catalyst; (b) Pt Ce (3 wt.%)/Al_2O_3 catalyst.

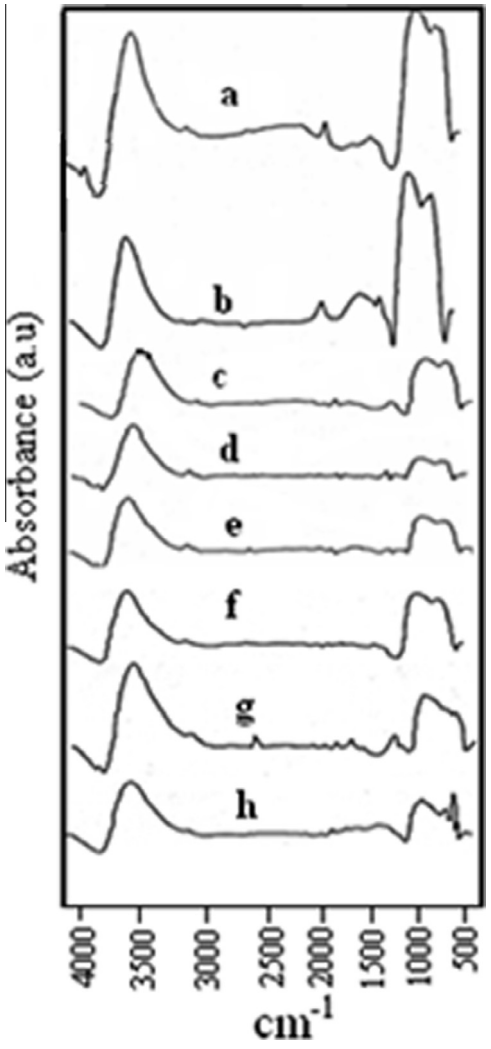

Figure 4 FTIR of: (a) Al_2O_3; (b) Pt/Al_2O_3; (c) Pt-La (0.25 wt.%)/Al_2O_3; (d) Pt-La (1.5 wt.%)/Al_2O_3; (e) Pt-La (3 wt.%)/Al_2O_3; (f) Pt-Ce (0.25 wt.%)/Al_2O_3; (g) Pt-Ce (1.5 wt.%)/Al_2O_3; (h) Pt-Ce (3 wt.%)/Al_2O_3.

tetrahedral coordinated alumina ion in a non vacant environment. The spectra of Pt/Al_2O_3 catalyst (Fig. 4b) exhibit the presence of a broad band in the range 1500–1000 cm^{-1} which are related to different electronic Pt species [18], indicating that Pt exists in several oxides species [19]. The vibration band at 3790 cm^{-1} has almost disappeared, after Pt loading, which indicates that loading of Pt has lowered the acidity of the alumina sample as some Pt particles fit into the Al_2O_3 pores and others present on the outer surface of the catalyst. However, the intensity of the bands associated to Al_2O_3 in the area of 1100–500 cm^{-1} has decreased upon loading by La and Ce (Fig. 4c–h). As Ce content increases, additional new bands appear in the region 1000–500 cm^{-1}(Fig. 4h) which indicate the presence of CeO_2 particles on the external surface of Al_2O_3 in accordance with DSC results verification (Fig. 2b). Accordingly, loading alumina by La_2O_3 has proved a strong interaction occurrence between the two elements that lead to a higher degree of La_2O_3 dispersion (Fig. 3c, d and e) that could be reflected by an increased basicity according to Kubota et al. [20]. Fig. 4 indicates changes in the frequencies of the bands 1500–1000 cm^{-1} which might lead to a change in electronic properties of Pt species leading to the formation of new Pt species.

3.1.5. H_2-TPR

Effects of the addition of La and Ce promoters on the reducibility of Pt/γ-Al_2O_3 catalyst were studied by H_2-TPR. (Fig. 5) As observed, all catalysts exhibit a sharp reduction peak around 730–700 °C which might be related to the reduction of contaminants in alumina support (Fig. 5a) [21]. The profile of the undoped monometallic catalyst Pt/Al_2O_3 (Fig. 5b) displays two reduction peaks, one near 314 °C which is explained as due to the reduction of Pt oxides that interact weakly with Al_2O_3 support and a second smaller one at about 500 °C that is due to the reduction of Pt oxides which interact strongly with the support and as reported by Damyanova and Bueno [23]. The TPR profiles of the ternary system (Pt CeO_2/Al_2O_3) are shown in (Fig. 5c–e). As denoted, the position of TPR peaks depends on the amount of CeO_2 and therefore on the type and strength of the interaction between supported Pt-oxide species and the alumina support. Previous studies concluded that the presence of ceria can strongly influence the oxidation and reduction properties of

supported noble metals [22]. While a peak shoulder appears near the first reduction peak of Pt-oxide species in the lower temperature region 225–250 °C (Fig. 5d and e) another peak appears at 475 and 450 °C at CeO_2 loading of 1.5 and 3 wt.%, respectively. The intensity of this peak increases with increasing of CeO_2 loading, confirming the presence of reduced surface ceria presence, indicating the influence of Pt on the surface of CeO_2-Al_2O_3 toward easier reduction of CeO_2. TPR profiles of the Pt La_2O_3/Al_2O_3 catalysts are shown in (Fig. 5f–h) indicating the addition influence of La_2O_3 on the state of pt and as revealed by FT-IR analysis.

3.1.6. H_2-TPD

Hydrogen is the one of the products of dehydrogenation reaction; accordingly its chemisorptions to the solid catalyst can strongly affect its performance. Utilizing H_2-TPD analytical tool would then shed some light on the disparity of metal/support interaction and electronic properties of supported metal particles [24]. Usually, low temperature desorption peaks are assigned to hydrogen by metallic Pt [25] and the high temperature desorption peaks are assigned to spillover hydrogen, strong chemisorbed hydrogen and hydrogen in subsurface layers of the platinum [26]. TPD of hydrogen adsorbed during reduction and cooling in flowing H_2 (Fig. 6) exhibits the performance of the promoter free and that added to Pt/Al_2O_3. As noted, Pt/Al_2O_3 catalyst exhibits two peaks at a maximum of 140 and 180 °C; which are attributed to chemisorbed hydrogen desorbing from the platinum particles [25]; two Gaussian peaks at 480 °C and a smaller one with a maximum at 380 °C. Upon addition of La and Ce promoter to the Pt/Al_2O_3 catalyst, the ability to absorb hydrogen was found to be increased especially in the high temperature range. Previous studies by Odd et al. [21] indicated that over Pt-Sn/Al_2O_3 catalyst, the high temperature adsorbed hydrogen aids in maintaining catalyst activity, most probably by reducing coking on the metal. The appearance of multiple TPD peaks is attributed to desorption of "re-adsorbed hydrogen" [27]. Fig. 6 shows a change in intensity of the lower temperature desorption peaks indicating that addition of Ce leads to changes in the electronic properties of Pt supported on Al_2O_3.

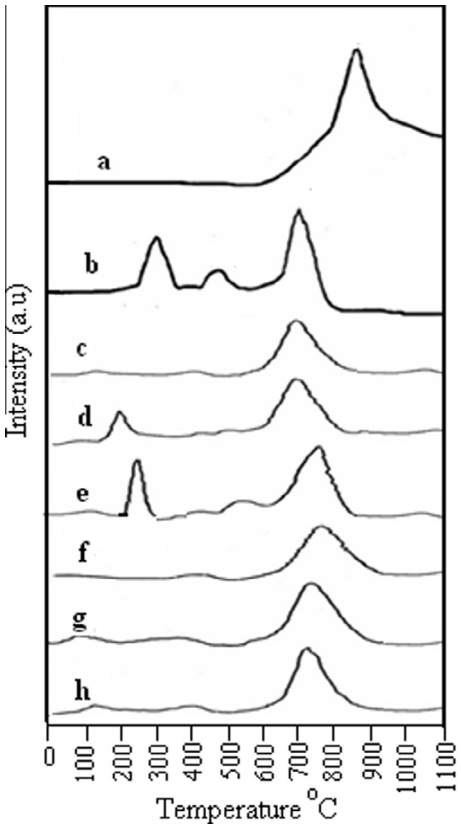

Figure 5 H_2-TPR profiles of: (a) Al_2O_3; (b) Pt/Al_2O_3; (c) Pt-Ce (0.25 wt.%)/Al_2O_3; (d) Pt-Ce (1.5 wt.%)/Al_2O_3; (e) Pt-Ce (1.5 wt.%)/Al_2O_3; (f) Pt-La (0.25 wt.%)/Al_2O_3; (g) Pt-La (1.5 wt.%)/Al_2O_3; (h) Pt-La (3 wt.%)/Al_2O_3.

3.1.7. CO_2-TPD

In order to explore such a relationship between the catalytic and basic properties of the catalyst samples a detailed investigation of basicity of these samples was carried out using TPD of CO_2. The number and strength of basic sites are evaluated from the intensity and position temperature of TPD signals, respectively, results of which are illustrated in Fig. 7. As can be seen, the strength of the basic sites decreases in the order Pt Ce/Al_2O_3 > Pt La/Al_2O_3, in addition to the increase of the basic strength as additive content is increased.

3.1.8. NH_3-TPD

To assess the acidity of the different catalysts NH_3-TPD adsorption/desorption behavior was followed. NH_3 desorption from Al_2O_3-based materials is usually reported in the range between 100 and 800 °C for NH_3 that is adsorbed on the acid sites (OH groups). Fig. 8 illustrates the influence of La_2O_3 and CeO_2 promoting results on the population of acidic sites and consequently on the amount of adsorbed NH_3. Pt/Al_2O_3

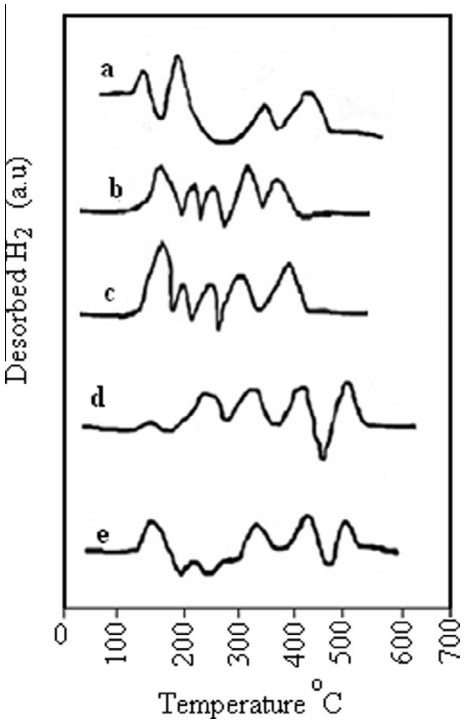

Figure 6 H_2-TPD profile of: (a) Pt/Al_2O_3; (b) Pt-La (0.25 wt.%)/Al_2O_3; (c) Pt-La (3% wt.%)/Al_2O_3; (d) Pt-Ce (0.25 wt.%)/Al_2O_3; (e) Pt-Ce (3% wt.%)/Al_2O_3.

presents the highest amount of NH_3 adsorbed on the catalyst, with two superimposed desorption peaks identified (~220 and ~325 °C), related to weak and medium/strong adsorbed NH_3. Upon introduction of La_2O_3 and CeO_2 a clear reduction of the desorbed NH_3 together with a significant shift to lower temperature for both the desorption maxima are observed indicating a reduction in the number and strength of the acidic sites of the catalysts aided by the very high dispersion of the promoting oxide on the alumina surface. The reduced acidity of the materials promoted by La_2O_3 and CeO_2 justify the performances of solid catalysts. Fig. 8 illustrate the NH_3-TPD profiles Pt/Al_2O_3 (a), Pt-La (3 wt.%)/Al_2O_3 (b) and Pt-Ce(3 wt.%)/Al_2O_3 (c) reduced at 500 °C.

3.1.9. HRTEM

To construct an overall preview of the effect of La and Ce promoters on the performance of Pt/Al_2O_3 during catalytic conversion of *n*-alkanes TEM studies of the solid particles were carried out. Fig. 9 illustrates the TEM images of the different solid catalysts. The TEM images indicate that the Pt particles appear as darker points in the lower nanosize range of 1–5.6 nm, while when the Pt particles supported over the alumina support their size increase to 3–5.6 nm. Nevertheless, a significant observation was noted when promoters are added where Pt particles are measured at 1.9–4.3 nm in the presence of either promoter, namely; La and Ce. It is also noted that the increase of La from 0.25 to 3 wt.% aided to decrease the particles size from 1.9–4.3 nm to 1.5–3 nm.

3.2. Catalytic conversion and selectivity

In the present work, the influence of the La, and Ce, as promoters, to the activity of Pt/Al_2O_3 during cyclohexane dehydrogenation, *n*-hexane and *n*-heptane dehydrocyclization reactions is analyzed using a pulsed catalytic microreactor.

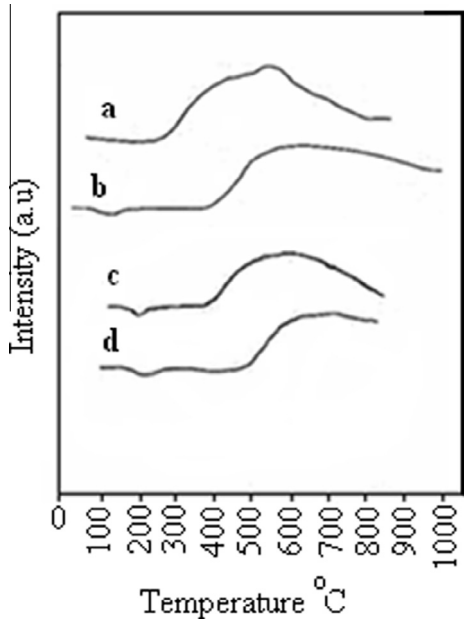

Figure 7 CO_2-TPD profile of: (a) Pt-La (0.25 wt.%)/Al_2O_3; (b) Pt-Ce (0.25 wt.%)/Al_2O_3/; (c) Pt-La (3 wt.%)/Al_2O_3; (d) Pt-Ce (3 wt.%)/Al_2O_3.

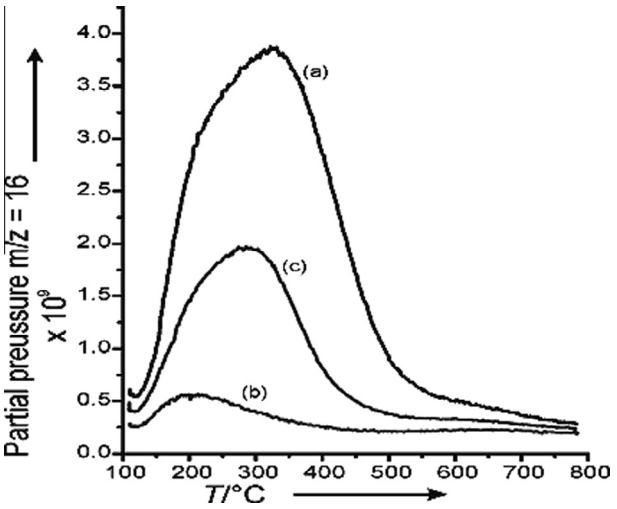

Figure 8 NH_3-TPD profiles recorded for the samples reduced at 500 °C: Pt/Al_2O_3 (a), Pt-La (3 wt.%)/Al_2O_3 (b) and Pt-Ce(3 wt.%)/Al_2O_3 (c).

The conversion (X) either by dehydrogenation or dehydrocyclization and selectivity (S) were calculated from the corrected integrated signals by:

$$X(\%) = \frac{I_{In} - I_{out}}{I_{In}} \times 100 \quad (1)$$

$$S(\%) = \frac{I_{product}}{I_{In} - I_{out}} \times 100 \quad (2)$$

where, the subscripts I_{In} and I_{out} represent the composition of components in the feed stream and in the product stream, respectively [30].

3.2.1. Dehydrogenation of cyclohexane

The catalytic conversion results are represented in Tables 2–4. The experimental results show that the conversion of cyclohexane is affected greatly by the reaction temperature, and that the activity of Pt/Al_2O_3 catalyst is higher than that shown by the promoted alumina (Table 4). The order of catalytic activities at all reaction temperatures for cyclohexane dehydrogenation to benzene with respect to the catalyst type is as follows: $Pt/Al_2O_3 > Pt\ La/Al_2O_3 < Pt\ Ce/Al_2O_3$. Table 3 shows that catalysts containing La_2O_3 exhibit higher activity for cyclohexane dehydrogenation than those containing CeO_2 (Table 4). As indicated by DSC results, the $Pt\ Ce/Al_2O_3$ samples show two crystalline structures of both γ-Al_2O_3 and ceria (Fig. 3). On the other hand we can see that for $Pt\ La/Al_2O_3$ samples $<\gamma$-Al_2O_3 phase is the only structure present. The formation of the γ-Al_2O_3 and CeO_2 structures in the ceria containing catalysts is an indication for the segregation of ceria. La_2O_3 segregation phenomenon is not observed, however, within the La containing samples. The formation of tetrahedral alumina when doped by La_2O_3 is considered as an additional support that the lanthanum is responsible for the modification of the alumina environment due to its incorporation and stabilization into the alumina network as revealed by Vazquez et al. [28]. FTIR and CO_2 analysis indicated that ceria containing catalysts are considered as basic oxides, which is considered as a disadvantage to dehydrogenation.

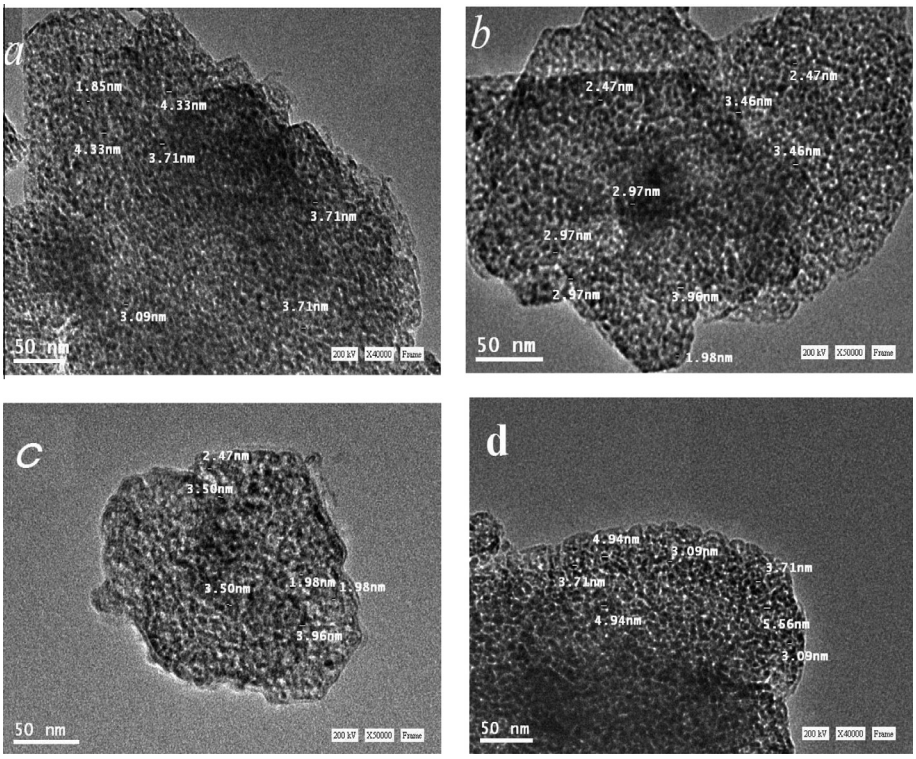

Figure 9 TEM images of: (a) Pt (0.35)La(0.25)/Al_2O_3; (b) Pt (0.35)La(3)/Al_2O_3; (c) Pt (0.35)La(0.25)/Al_2O_3; (d) Pt(0.35)/Al_2O_3.

3.2.2. Dehydrocyclization of n-heptane

Comparing cyclohexane dehydrogenation data, it can be seen that the Pt La/Al_2O_3 catalysts, possess higher dehydrogenation activity than the other promoted catalysts. These catalysts appeared to be more resistant to thermal treatment than the base Pt/Al_2O_3 catalyst as indicated by DSC analysis, Fig. 2. With regard to product distribution as a function of catalyst type, toluene was found as the major aromatic product in addition to heptane, methylcyclohexane and ethylcyclopentane. Benzene and methane are produced as probably due to hydrogenolysis by product. Table 5 exhibits the appearance of toluene which is formed probably through a consecutive process in which the intermediates are adsorbed species that quickly transform on the same active site of the catalyst surface from n-heptane to toluene as indicated by Davis [29]. Benzene and methane yield continuously grows up by increasing La content which might be formed as a secondary and final product from toluene by hydrogenolysis of its lateral chain as indicated Adolfo et al. [30]. In addition, formation of methylcyclohexane and ethylcyclopentane are might formed via direct cyclization of *n*-heptane in two possible parallel reactions, namely; C_1–C_6 and C_1–C_5 ring closure, respectively. Both reactions are claimed, although the 1,6-cyclization is more favored, at least over platinum [31] on non acid supports (non chlorinated alumina) at the temperature followed in the present work. Direct cyclization of C_1–C_6 might have occurred via ring closure of heptatrienes to methylcyclohexandiene. Skeletal isomerization takes place by hydrogenolysis of ethylcyclopentane and to a smaller extent by a bond-shift process [32]. In all experiments, the reaction product included a small concentration of *n*-heptene, which is considered as an intermediate during the formation of toluene from *n*-heptane by dehydrogenation on Pt metal and as reported by Lafyatis et al. [33].

Table 2 Cyclohexane dehydrogenation by using Pt/Al_2O_3 catalysts as a function of reaction temperature.

Catalyst	Pt/Al_2O_3			
Temperature (°C)	300	350	400	450
Conversion (wt.%)	47	60	72	78
Benzene	47	60	64	66
n-Hexane	—	—	8	12
Selectivity (wt.%)				
Benzene	100	100	88.9	91.7
n-Hexane	—	—	11.1	8.3

3.2.2.1. n-Heptane dehydrocyclization mechanism. According to the above results and mechanistic elucidation, *n*-heptane is transformed over the Pt/Al_2O_3 and La promoted catalysts through a complex network of parallel and consecutive interconnected reactions as suggested in Scheme 1, with intermediate compounds [30], the overall chemical process occurs on the catalyst surface, involving adsorbed species (σi). The pathway includes reaction of cyclization (CY), dehydrogenation (DH), isomerization (IS) and hydrogenolysis (HL).The initial stage of the mechanism is the adsorption of *n*-heptane through its terminal carbon atom (C_1) on a metallic center, with abstraction of a hydrogen atom by other neighboring metallic centers, giving the first reactive intermediate species (σC_7). Heptenes and methylcyclohexane have been identified as precursors of

Table 3 Cyclohexane dehydrogenation by using PtLa/Al_2O_3 catalysts as a function of reaction temperature.

Catalyst	Pt La(0.25 wt.%)/Al_2O_3				Pt La(1.5 wt.%)/Al_2O_3				Pt La(3 wt.%)/Al_2O_3			
Temperature (°C)	300	350	400	450	300	350	400	450	300	350	400	450
Conversion, wt.%	34	47	58	63	39	51	60	64	43	55	62	65
Benzene	34	47	53	55	39	51	57	59	43	55	62	65
n-Hexane	–	–	5	8	–	–	3	5	–	–	–	–
Selectivity, wt.%												
Benzene	100	100	91.4	87.3	100	100	95	92.2	100	100	100	100
n-Hexane	–	–	8.6	12.7	–	–	5	7.8	–	–	–	–

Table 4 Cyclohexane dehydrogenation by using Pt Ce/Al_2O_3 catalysts as a function of reaction temperature.

Catalyst	Pt Ce(0.25 wt.%)/Al_2O_3				Pt Ce(1.5 wt.%)/Al_2O_3				Pt Ce(3 wt.%)/Al_2O_3			
Temperature °C	300	350	400	450	300	350	400	450	300	350	400	450
Conversion, wt.%	24	40	46	52	32	44	55	58	36	48	60	66
Benzene	24	36	40	42	32	44	52	52	36	48	60	66
n-Hexane	–	4	6	10	–	–	3	6	–	–	–	–
Selectivity, wt.%												
Benzene	100	90	87	80.8	100	100	94.5	89.7	100	100	100	100
n-Hexane	–	10	13	19.2	–	–	5.5	10.3	–	–	–	–

Table 5 *n*-Heptane dehydrocyclization at 450 °C by using Pt La/Al_2O_3 as a function of La content and Pt /Al_2O_3 catalysts.

n-Heptane dehydrocyclization	Catalyst type			
	Pt La(0.25 wt.%)/Al_2O	Pt La(1.5 wt.%)/Al_2O_3	Pt La(3 wt.%)/Al_2O_3	Pt/Al_2O_3
Conversion, wt.%	33	63	97	91
Methane	—	1	2	4
n-Heptene	2	5	9	5
Ethylcyclopentane	3	4	4	4
Methylcyclohexane	18	23	28	18
Benzene	—	7	15	27
Toluene	10	23	39	33
Selectivity, wt.%				
Methane	—	1.6	2	4.4
n-Heptene	6	8	9.3	5.5
Ethylcyclopentane	9	6.4	4.0	4.4
Methylcyclohexane	54.5	36.5	29	19.8
Benzene	—	11	15.5	29.7
Toluene	30.5	36.5	40.2	36.2

toluene and they are transformed faster than *n*-heptane on the catalyst surface. From this C_1 adsorbed entity, the different paths of the network are determined by the position of the second adsorbed carbon atom in the chain of the σC_7. Results revealed in Table 5 show that heptene, appears as a precursor of methylcyclohexane. Thus, it is reasonable to assume that the subsequent adsorption of the C_2 carbon atom on Pt with the formation of the first alkene-like intermediate ($\sigma C_7^=$) should be highly favored, in agreement with the most published results [29].

This species may be transformed following different routes, namely:

i- Desorption to the gas phase as heptane.

ii- C_1–C_6 ring closure with formation of methylcyclohexane, which may desorb to the gas phase or successively dehydrogenate on the surface to give finally toluene (Path I). This path is very feasible due to the high aromatizing selectivity of the Pt/Al_2O_3 catalyst, which could have be enhanced by the addition of La_2O_3, which increases the reducibility of platinum as evidenced by TPR analysis (Fig. 5).

iii- The species $\sigma C_7^=$ may be successively dehydrogenated to heptatriene ($\sigma C_7^=$) (Path II) and then undergo cyclization to toluene. Eventually, cyclization of the alkene and/or alkadiene adsorbed species may give the

corresponding adsorbed cycle of the path I. It should be noted that neither heptadienes nor heptatriene were detected in the product, indicating that the reactivity of these intermediates is so high that they react before they desorb, in accordance to the literature data [33].

iv- C_1–C_5 closure with formation of ethylcyclopentane, which may desorb to the gas phase or give rise to different types of compounds and, indirectly, can also lead to toluene (Paths III of the scheme). To meet the Tee principle [34] the appearance of toluene as a primary product can be explained assuming that the successive transformations, of the intermediates in paths I and II take place in the adsorbed phase, on the same active site, following the mechanism in the literature data [34]. In this mechanism, the intermediates methylcyclohexane and heptenes formed are stable molecules, which can desorb to the gas phase. In contrast, the highly unsaturated adsorbed intermediates are too reactive to be desorbed and appearing between reaction products. Experimental evidences of the dehydrocyclization mechanism via unsaturated intermediates have been also discussed in earlier publications [34]. It is important to point out, on the other hand, that the mechanism in Scheme 1 is proposed on the basis of results obtained at atmospheric pressure, because at higher pressures it may be different.

3.2.3. Dehydrocyclization of n-hexane

It has been demonstrated that Pt La (3 wt.%)/Al_2O_3 was the best catalyst for *n*-heptane dehydrocyclization. Aromatization of *n*-hexane is more difficult than that of higher hydrocarbons. [35] An attempt to explain this property is made here, by a comparative study on the mentioned catalyst and Pt/Al_2O_3. Two catalysts have been compared in a pulse system at 450 °C as in *n*-heptane aromatization reaction. Inspecting Table 6 we observe that the presence of La_2O_3 leads to double

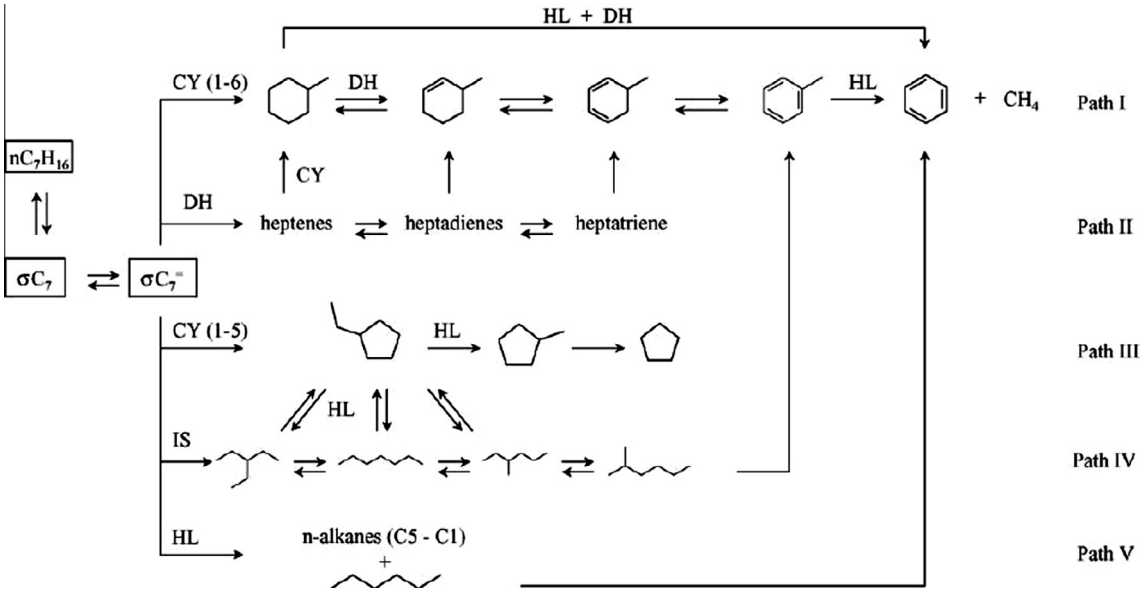

Scheme 1 Reaction pathway for dehydrocyclization of *n*-heptane [30].

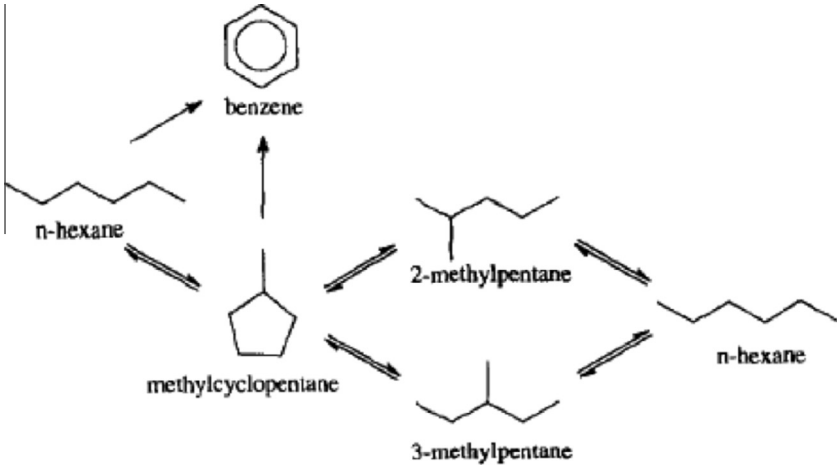

Scheme 2 *n*-Hexane dehydrocyclization mechanism [36].

Table 6 *n*-Hexane dehydrocyclization at 450 °C by using Pt/Al_2O_3 and Pt La(3 wt.%)/Al_2O_3 catalyst.

n-Hexane dehydrocyclization	Catalyst	
	Pt/Al_2O_3	Pt La(3 wt.%)/Al_2O_3
Conversion, wt.%	64.5	71
Methylcyclopentane	34.5	12
Benzene	30	59
Selectivity, wt.%		
Methylcyclopentane	53.5	17
Benzene	46.5	83

benzene formation from 30 to 59% and selectivity was also modified from 46.5 to 83%. The aromatization of *n*-hexane to benzene is accompanied by the formation of methylcyclopentane. Table 6 shows the absence of cyclohexane as a product, explaining that it is completely converted into benzene. It is reasonable to expect that the effect of La_2O_3 during aromatization is different for the two reactions studied here: *n*-hexane to benzene and cyclohexane to benzene, although the end-product is the same. This indicates that the promotion of aromatization had no effect on the dehydrogenation of cyclo-alkane, but rather an effect on the ring closure. Dehydrogenation of cyclohexane to benzene is a reaction which occurs on the freely exposed platinum surface. Suppression of the activity in dehydrogenation of cyclohexane on Pt/Al_2O_3 promoted catalysts points to a blocking and ensemble size effects, respectively. The effect on aromatization is then clearly a promotion effect which prevails over the blocking effect as indicated by Fukunaga and Ponec [36].

3.2.3.1. n-Hexane dehydrocyclization mechanism. The aromatization of *n*-hexane to benzene goes by the ring closure, which proceeds either via a stepwise dehydrogenation (*n*-hexane–hexene–hexadiene–hexatriene) or via intermediates bound to the surface by a carbon-like or carbine-like bonds, possibly in combination with a π-complexing of the olefinic bond in the intermediate [37]. Manninger et al. [38] expressed a very interesting view that the presence of alkali cations can influence the formation of the intermediates adsorbed on Pt; considered as a sterical or electronic field effect. The aromatization of *n*-hexane to benzene is accompanied by the formation of methylcyclopentane, which is then dehydroisomerized into benzene (Scheme 2). The methylcyclopentane is formed directly on the metal sites by a 1,5 ring closure rather than by an acid catalyzed isomerization of cyclohexane as indicated by Shum et al. [39] Also cyclohexane was not detected in the product indicating that it is converted completely into benzene.

4. Conclusions

In this study several catalysts of platinum supported on γ-Al_2O_3 promoted with Ce, and La oxides were prepared as functional catalysts for the dehydrocyclization of alkanes. Catalytic cyclohexane dehydrogenation, *n*-hexane and *n*-heptane dehydrocyclization were carried out with regard to the type and concentration of the promoter. Results of cyclohexane dehydrogenation indicate that the reaction selectivity decreases upon the addition of the promoters to Pt/Al_2O_3 catalyst that may be related to a geometric or electronic modification of the active Pt particles, as indicated by FTIR, H_2-TPD, and H_2-TPR analysis.

Moreover, the activity loss of La and Ce containing catalysts, related to the reduction of the number and strength of the acidic sites present on the catalyst surface as indicated by NH_3-TPD analysis, which is one of the disadvantages of the dehydrogenation. The significantly lower acidity of the La_2O_3-based system can be associated with the very high dispersion of the promoting oxide on the alumina surface as indicated by DSC and FTIR. Segregation phenomena are not observed employing La_2O_3 containing catalyst confirming γ-Al_2O_3 as the stabilized structure presence while segregation in presence of cerium oxide was observed.

The effect of the presence of promoters on aromatization is very different for the two reactions studied, namely; cyclohexane to benzene and *n*-hexane to benzene, although the end-product was found to be the same. Such observation indicates that the promotion of the aromatization is not an effect of the dehydrogenation of cyclo-alkane, but rather an effect of ring closure. The presence of La_2O_3 within the Pt/Al_2O_3 catalyst proved promotion of aromatization of *n*-hexane and *n*-heptane. Aromatization of *n*-hexane is more difficult than that of *n*-heptane. Pt La (3 wt.%)/Al_2O_3 catalyst appeared to be more active, more selective toward aromatization and more thermally resistant than the basic Pt/Al_2O_3 catalyst. Thus modification of the Pt/Al_2O_3 catalyst by La_2O_3 results in a catalyst with altered activity and selectivity being more active and selective reforming of catalyst.

References

[1] J.T. Michael, C. Sun, Naphtha cracking for light olefins production, Petroleum Technology Quarterly Q3 (Jul, Aug, Sep.), 2010, pp. 87–91.
[2] W. Zhang, L. Li, Y. Du, X. Wang, P. Yang, Catal. Lett. 127 (2009) 429–436.
[3] B. Zhao, C.J. Chou, Y.W. Chen, Ind. Eng. Chem. Res. 49 (2010) 1669–1676.
[4] M. Iwasaki, H. Shinjoh, Chem. Commun. 47 (2011) 3966–3968.
[5] H. Shinjoh, J. Alloys Compd. 408–412 (2006) 1061–1064.
[6] X. Fang, F. Li, Q. Zhou, L. Luo, Appl. Catal. A. 161 (1997) 227–234.
[7] A. Furch, A. Tungler, S. Szabo, A. Sarkani, Appl. Catal. A. 226 (2002) 155–161.
[8] K.A.-G. Ahmed, E.A. Ahmed, A.K.A.-G. Noha, A.S. El-Sayed, A.A. Mohammed, Appl. Catal. A. 334 (2008) 304–310.
[9] C. Yu, Q. Ge, H. Xu, W. Li, Appl. Catal. A. 315 (2006) 58–61.
[10] S. Damyanova, C.A. Perez, M. Schmal, J.MnC. Bueno, Appl. Catal. A 234 (2002) 271–282.
[11] D. Tichit, M. Lhouty, A. Guida, B. Chiche, F. Figueras, A. Autoroux, D. Bartalini, E. Garron, J. Catal. 151 (1995) 50–59.
[12] L. Gouran, L. Wei, Z. Minghui, T. Keyi, Catal. Today 93–95 (2004) 595–601.
[13] M. Dan, M. Mihet, A.R. Biris, P. Marginean, V. Almasan, G. Borodi, F. Watanabe, A.S. Biris, M.D. Lazar, React. Kinet. Mech. Catal. 105 (2012) 173–193.
[14] J. Erena, I. Sierra, M. Olazar, G. Gayubo, A.T. Aguayo, Ind. Eng. Chem. Res. 47 (2008) 2238–2247.
[15] S. Srinivasan, C.R. Narayanan, A.K. Datye, Appl. Catal. A 132 (1995) 289–308.
[16] C. Ma, Y. Chang, W. Ye, W. Shang, C. Wang, J. Colloid Interface Sci. 317 (2008) 148–154.
[17] J.M. Saniger, Mater. Lett. 22 (109) (1995) 109–112.

[18] A. Arcoya, X.L. Seoane, J.M. Grau, Appl. Surf. Sci. 205 (206) (2003) 206–211.
[19] J. Oi-Uchisawa, S. Wang, T. Nanba, A. Ohi, A. Obuchi, Appl. Catal. B 44 (2003) 207–215.
[20] Y. Sugi, Y. Kubota, K. Komura, N. Sugiyama, M. Hayashi, J.-H. Kim, G. Seo, Appl. Catal. A 299 (2006) 157–166.
[21] A.B. Odd, H. Anders, A.B. Edd, J. Catal. 158 (1996) 1–12.
[22] S.A. Bocaregra, S.R. De Miuel, I. Borbath, J.L. Margiffalvi, O.A. Scalza, J. Mol. Catal. A. Chem. 301 (52) (2009) 52–60.
[23] S. Damyanova, J.M.C. Bueno, Appl. Catal. A 253 (2003) 135–150.
[24] S. Jujjuri, E. Ding, E.L. Hommel, S.G. Shore, M.A. Keane, J. Catal. 239 (2006) 486–500.
[25] J.T. Miller, B.L. Meyers, F.S. Modica, G.S. Lane, M. Vaarkamp, D.C. Koningsberger, J. Catal. 143 (1993) 395–408.
[26] J.T. Miller, B.L. Meyers, M.K. Barr, F.S. Modica, D.C. Koningsberger, J. Catal. 159 (1996) 41–49.
[27] F. Benseadj, F. Sadi, M. Chater, Appl. Catal. A 228 (2002) 135–144.
[28] A. Vazquez, T. Lopez, R. Gomez, X. Bokhimi, J. Mol. Catal. A 167 (2001) 91–99.
[29] B.H. Davis, Catal. Today 53 (1999) 443.
[30] A. Adolfo, L.S. Xose, M.G. Javier, Appl. Catal. A. 284 (2005) 85–95.
[31] B.H. Davis, P.B. Venuto, J. Catal. 15 (1969) 363–372.
[32] H. Pines, L. Nogueira, J. Catal. 70 (391) (1981) 391–403.
[33] D.S. Lafyatis, G.F. Froment, A. Pasauclaerb-out, E.G. Derouane, J. Catal. 147 (1994) 552–566.
[34] O.S. Tee, J. Am. Chem. Soc. 91 (7144) (1969) 7144–7149.
[35] G. Centi, R.W. Joyner, R.A. Van Santen (Eds.), Elementary Reaction steps in Heterogeneous catalysis, vol. 93, Kluwer Academic Publishers, Dordrecht, The Netherlands, 1993.
[36] T. Fukunaga, V. Ponec, Appl. Catal. A 154 (1997) 207–219.
[37] Z. Paal, J. Catal. 105 (1987) 540–542.
[38] I. Manninger, Z. Zhan, X.L. Xu, Z. Paal, J. Mol. Catal. 66 (1991) 223–237.
[39] V.K. Shum, J.B. Butt, W.M.H. Sachtler, Appl. Catal. 11 (1984) 151–154.